Available online at www.sciencedirect.com
SCIENCE DIRECT®
Journal of Sound and Vibration 292 (2006) 443–460
JOURNAL OF SOUND AND VIBRATION
www.elsevier.com/locate/jsvi

Understanding the occurrence of squealing noise using the temporal finite element method

L. Baillet[a,*], S. D'Errico[a], B. Laulagnet[b]

[a]*INSA Lyon, Contact and Solid Mechanics Laboratory (LaMCoS), 69621 Villeurbanne Cedex, France*
[b]*INSA Lyon, Vibration–Acoustics Laboratory (LVA), 69621 Villeurbanne Cedex, France*

Received 16 November 2003; received in revised form 27 July 2005; accepted 2 August 2005
Available online 19 September 2005

Abstract

This paper focuses on the vibration phenomena involved during friction contact and which lead to squealing noise. The simulation uses an explicit dynamic finite element method to describe the vibration of a pad brought into contact with a beam at constant velocity. In particular it describes a study on the influence of certain parameters on the occurrence of instability on pad and beam vibration. These parameters are beam velocity, the external force applied to the pad, the Coulomb friction coefficient, the pad's dimensions and Young modulus. The mechanism leading to the occurrence of squealing noise and unstable pad mode causing the onset of instability are shown. The vibration structure displays periodic peaks corresponding to the occurrence of impacts at the interface generated by steady-self pulse propagation.

1. Introduction

The specific characteristics expected of brakes are a high and stable friction coefficient, low disc wear and low pad wear. During braking, special attention is given to vibration that could be the source of excess stress and noise. Noise, up till now hidden by background noise, is currently a major field of automobile and railway research. Squealing noise is a high frequency vibration

*Corresponding author. Fax: +33 4 78 89 09 80.
E-mail addresses: laurent.baillet@insa-lyon.fr (L. Baillet), bernard.laulagnet@insa-lyon.fr (B. Laulagnet).

0022-460X/$ - see front matter © 2005 Published by Elsevier Ltd.
doi:10.1016/j.jsv.2005.08.001

(1–20 kHz) characterized by a pure and strident sound of strong intensity that has been the subject of much research. However, little is known about the friction mechanisms that start in the braking system or the different couplings that link the elements of the "tribological triplet" [1–3], namely the mechanism formed by the two first bodies in contact and the third body, composed of wear particles trapped in the contact. These elements enable us to understand and predict the source of the noise. Brake squealing is due to the occurrence of dynamic instability generated at the surface of the two bodies in friction. Different theories and models have been proposed that rely on phenomena such as the "stick–slip" phenomenon, which was the first type of instability to be discovered [4]. Modal studies have been performed [5–7], some of which have dealt with the "sprag–slip" phenomenon [8–13]. These models, which have one or many degrees of freedom, are used to explain and simulate the occurrence of dynamic instability. Akay [14] has reviewed the work carried out on vibrations caused by friction between two bodies in relative movement. Moreover, Adams [15,16], Simões [17], and Rice [18,19] have analysed the presence of instabilities characterized by the existence of steady-self pulses on the contact surface. They have shown that two bodies in contact and in relative movement can display dynamically unstable behaviour expressed in the form of waves propagating on the interface zone of the two bodies. These waves depend on the characteristics of the two bodies in contact. Applied load and velocity are important parameters of the system's behaviour. Nguyen [20] and Oueslati [21,22] performed a numerical 2D study of the transition of the response of a dry Coulomb contact into a steady-self pulse solution that takes the form of stick–slip–separation waves propagating on the contact surface.

This paper describes the use of a finite element simulation, based on the laboratory's PLAST3 code in explicit dynamic formulation, to study the instabilities at the contact zone of the two bodies in friction. We focus in particular on the coupling between the two first bodies (pad and beam) and the third body which is taken into account in the simulations by a Coulomb friction coefficient. The models considered and analysed are simplifications of a complete braking system [23]. The disc/pad braking system has been replaced by a model with a beam and a parallelepiped body (pad) (Fig. 1). This study presents the influence of the following parameters: Young's modulus, velocity, pad dimensions, force applied to the pad, friction coefficient, occurrence of instabilities. The results were subjected to time and frequency analysis and show that the

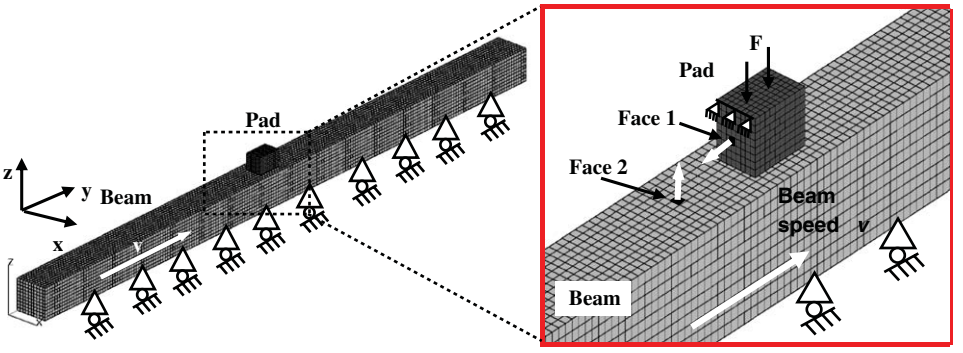

Fig. 1. Finite element simulation of pad friction on a moving beam.

characteristics of the acceleration spectra are periodic in frequency while their harmonic range is linked to separation between the pad and beam contact surfaces.

2. PLAST3 formulation

PLAST3 in (3D) [24,25], an explicit dynamic finite element code, is used to simulate the behaviour of the first bodies (pad and beam) during frictional contact. PLAST3 is designed for large deformations and nonlinear material behaviour and uses a forward Lagrange multiplier method [26] for the contact between deformable bodies. For the dynamic study, the formulation is discretized spatially by using the finite element method and discretized temporally by using the β_2 method. The contact algorithm uses slave nodes (situated on the pad contact surface) and target surfaces (on the beam) described by four-node quadrilateral elements, since the 3D element used is an isoparametric hexahedra. An elementary target surface defined by four nodes is broken down into a bi-cubic Ferguson patch with C^1 continuity across the adjacent boundary [23].

The equation of the forward increment Lagrange multiplier method is constructed using equations of motion developed via the principle of a virtual work equation at time step t_n ($t_n = n\Delta t$) and the displacement constraints acting on the surfaces in contact at time t_{n+1}

$$\begin{aligned} &\mathbf{M}\ddot{\mathbf{u}}_n + \mathbf{K}\mathbf{u}_n + \mathbf{G}_{n+1}^{\mathrm{T}}\boldsymbol{\lambda}_n = \mathbf{r}_n, \\ &\mathbf{G}_{n+1}\{\mathbf{x}_n + \mathbf{u}_{n+1} - \mathbf{u}_n\} \leqslant \mathbf{0}, \end{aligned} \tag{1}$$

where $\boldsymbol{\lambda}_n$ is the contact force vector acting on the nodes of the slave surface, $\mathbf{G}_{n+1}$ is the global assembled matrix of the elementary matrices of the constraints, $\mathbf{x}_{n+1} = \mathbf{x}_n + \mathbf{u}_{n+1} - \mathbf{u}_n$ is the coordinate vector at time t_{n+1}, $\mathbf{M}$ is the mass matrices, and $\mathbf{r}_n$ is the nodal vectors of external forces. At any time step, the velocity $\dot{\mathbf{u}}_n$ and acceleration $\ddot{\mathbf{u}}_n$ vectors are related to displacements and time increment Δt in accordance with the β_2 method ($\beta_2 \in [0.5; 1]$)

$$\begin{aligned} \ddot{\mathbf{u}}_n &= \frac{2}{\Delta t^2}(\mathbf{u}_{n+1} - \mathbf{u}_n - \Delta t\dot{\mathbf{u}}_n), \\ \dot{\mathbf{u}}_n &= \frac{1}{1+2\beta_2}\left\{\dot{\mathbf{u}}_{n-1} + \Delta t(1-\beta_2)\ddot{\mathbf{u}}_{n-1} + \frac{2\beta_2}{\Delta t}(\mathbf{u}_{n+1} - \mathbf{u}_n)\right\}. \end{aligned} \tag{2}$$

The classical central difference scheme can be found by $\beta_2 = 0.5$.

The new coordinates $\mathbf{x}_{n+1}^* = \mathbf{x}_n + \mathbf{u}_{n+1}^* - \mathbf{u}_n$ of the nodes situated on the contact surface (pad and beam) are first computed with $\boldsymbol{\lambda}_n$ being equal to zero. If $\beta_2 = 0.5$, the nodal displacements at time t_{n+1}^* are obtained so that:

$$\mathbf{u}_{n+1}^* = \Delta t^2\mathbf{M}^{-1}(\mathbf{r}_n - \mathbf{K}\mathbf{u}_n) + 2\mathbf{u}_n - \mathbf{u}_{n-1}. \tag{3}$$

An elementary constraint matrix is formulated for each slave node that has penetrated through a target surface. The global assembled matrix $\mathbf{G}_{n+1}$ permits calculating contact forces $\boldsymbol{\lambda}_n$ and coordinates $\mathbf{x}_{n+1}$:

$$\begin{aligned} \boldsymbol{\lambda}_n &= \{\Delta t^2\mathbf{G}_{n+1}\mathbf{M}^{-1}\mathbf{G}_{n+1}^{\mathrm{T}}\}^{-1}\mathbf{G}_{n+1}(\mathbf{x}_n + \mathbf{u}_{n+1}^* - \mathbf{u}_n), \\ \mathbf{u}_{n+1} &= \mathbf{u}_{n+1}^* - (\Delta t^2\mathbf{M}^{-1}\mathbf{G}_{n+1}^{\mathrm{T}}\boldsymbol{\lambda}_n). \end{aligned} \tag{4}$$

Eqs. (4) are solved using the Gauss–Seidel method. During each internal iteration of this method, as no bonding and a standard Coulomb friction law are considered on each pad slave node, the contact conditions are expressed as

$$\begin{aligned} &\boldsymbol{\lambda}_n^{\mathbf{n}} \leqslant 0 \quad \text{(contact)},\\ &||\boldsymbol{\lambda}_n^{\mathbf{t}}|| \leqslant \mu|\boldsymbol{\lambda}_n^{\mathbf{n}}|,\\ &\quad \text{if } ||\boldsymbol{\lambda}_n^{\mathbf{t}}|| < \mu|\boldsymbol{\lambda}_n^{\mathbf{n}}|, \quad v_t = 0 \ \text{(stick)},\\ &\quad \text{if } ||\boldsymbol{\lambda}_n^{\mathbf{t}}|| = \mu|\boldsymbol{\lambda}_n^{\mathbf{n}}|, \quad \boldsymbol{\lambda}_n^{\mathbf{t}} \cdot v_t \leqslant 0 \ \text{(slip)}, \end{aligned} \tag{5}$$

where v_t is the relative tangential velocity of a slave node related to the target surface, and $\mathbf{n}$ and $\mathbf{t}$ are the normal and tangential vectors defining the contact. The friction law used is the standard Coulomb friction model without regularization of the tangential stress. It should be noted that in their work, Ranjith [19] and Simões [17] used a regularized law.

The vibratory mechanisms must take into account the damping phenomena internal to the beam and pad materials. These are introduced by assuming that they behave linearly and obey "viscoelasticity" laws. The tensor of the viscoelastic stress is thus linked to the deformation tensor by Hooke's law, generalized on the basis of a homogeneous and isotropic material:

$$\boldsymbol{\sigma} = \mathbf{D}\,\boldsymbol{\varepsilon} + \beta_v \mathbf{D}\,\frac{\mathrm{d}\boldsymbol{\varepsilon}}{\mathrm{d}t}, \tag{6}$$

where $\mathbf{D}$ represents the matrix of the material behaviour which, in an isotropic and homogeneous case, depends only on Young's modulus E and Poisson's ratio v. $\boldsymbol{\varepsilon}$ represents the deformation tensor. Coefficient β_v is a characteristic of the material viscosity and can be obtained experimentally.

3. Pad/beam contact simulation

The PLAST3 code allows us to analyse the instability generated in the contact between the two bodies (pad and beam) during friction as well as the level of acceleration generated. Mathematically, this instability is associated with the amplification of small perturbations from uniform steady sliding to large oscillations that destabilize the steady-state motion. In this paper, only the results of acceleration will be presented, with the assumption that the temporal and frequential behaviour of the acceleration is a good indicator of the noise emitted. Laulagnet [27] presents further developments concerning vibroacoustic transfer mechanisms. Initially, an increasing force F is applied in direction z until it reaches a pre-selected value in order to correspond to a uniformly normal displacement (along z) on the top of the pad (Fig. 1). Application of this force brings the pad into frictional contact with the beam moving at constant applied speed v. This speed is imposed according to y at the lower nodes of the beam.

The two deformable bodies are meshed with 3D hexahedral elements with smooth surfaces (roughness and superficial imperfections are neglected), while no account is taken of thermal and physicochemical effects. The characteristics of the two bodies (pad and beam) in contact are given in Table 1.

Table 1
Beam and pad characteristics

Beam	
Young's modulus E (MPa)	210 000
Poisson's coefficient v	0.3
Density ρ (kg/m^3)	8000
Width(x) × length(y) × height(z) (mm)	$20 \times 400 \times 20$
Pad	
Young's E modulus (MPa)	7000
Poisson's coefficient v	0.3
Density ρ (kg/m^3)	2500
Width(x) × length(y) × height(z) (mm)	$10 \times 30 \times 20$
Theoretical contact surface S (mm^2)	300

The boundary conditions under consideration are as follows:

- normal force F is applied to all the nodes of the upper surface of the pad; it is applied linearly at the beginning of the simulation, and stays constant thereafter;
- the nodes of the first line of the pad's upper surface are constrained along axes x and y;
- the lower nodes of the beam are constrained along axis z and their speed v is imposed according to y.

With the code in explicit dynamic formulation, the chosen time step Δt is smaller than the critical time step, which depends on Young's modulus E, Poisson's ratio v, density ρ, damping and on the length of the mesh elements of the bodies. The aim of these simulations is to show the influence of each parameter (Young's modulus, speed, friction coefficient μ, force applied and dimension of the pad) on distinctive scales such as local contact pressure, the kinematics of the contact surfaces of the two bodies and their acceleration (Fig. 1). Analysis of the latter will enable us to identify the frequencies at which these vibrations occur and know whether frequential components exist in the audible range (under 20 kHz). Since acoustic radiation is proportional to normal nodal acceleration, the latter is therefore presented in the temporal and frequential domains.

4. Results

4.1. Steady-self pulses

The simulations using the parameters described in Tables 1 and 2 showed instabilities on the contacting surface of the pad. The model enabled us to highlight the existence of steady-self pulse solutions in the form of stick–slip–separation, and stick–slip or slip–separation waves propagating on the contact surface [15,16,21,22,28,29]. These instabilities on the contact surface are the source of vibrations in the mechanism and thus one of the sources of the noise. A stable state is characterized by a contact surface where the pad nodes do not separate but remain in sliding contact on the moving beam. An unstable state is characterized by the formation on the pad

Table 2
Simulation parameters

Friction coefficient of the Coulomb type μ	0.5
Normal force applied to the pad F (N)	135
Theoretical pressure ($P_{th} = F/S$) (MPa)	0.45
Beam speed v (m/s)	5
Time step of the simulation Δt (s)	0.025×10^{-6}
Viscous damping β_v	0.5×10^{-6}

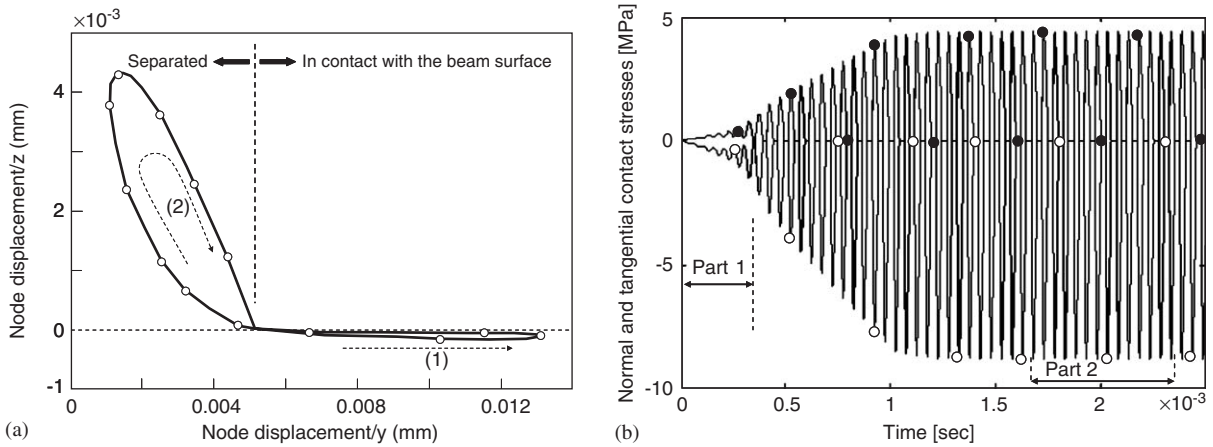

Fig. 2. (a) Trajectory; (b) ○ normal and ● tangential stresses of a node on the pad contact surface.

surface of sliding or sticking contact zones or zones separated from the beam surface. In the case where the state is "unstable", a time period related to the distribution of the mechanical volume and surface magnitudes is established. The periodic steady state will be dealt with later in the paper.

Fig. 2a shows the trajectory in the y–z plane of a node situated on the contact surface of the pad. This trajectory is composed of part (1) in which the node is in sliding or sticking contact in the direction of the movement. Part (2) is in the direction opposing the movement and corresponds to an elastic return where the node, initially in contact, separates from the beam surface. As the friction coefficient and beam speed are constant, the sliding or sticking of a zone depends on, among other things, the variation of the normal contact stress due to wave propagation, called dynamic effect [29]. The friction coefficient and beam speed are parameters that determine instabilities related to the coupling between tangential and normal motion. They are characterized in the model presented here by the separation or sticking of certain zones of the pad surface to or from zones of the beam. Threshold values exist for given friction coefficients and linear speeds above which a periodic steady state (unstable) is generated. This consideration agrees with the theories of Murakami [13], Eriksson [30,31] and Hultén [6,7] who have shown the existence of a friction coefficient threshold value above which squealing occurs. This periodic

steady state is characterized by steady-self pulses propagating in the direction of slip in the more compliant material, in this case the pad [32,33]. These pulses correspond to traction/compression stresses in the sliding direction and generated at a speed close to that of the material with the lower shear wave-speed. Normal contact stress at the contact can (Fig. 2b) therefore reach values 20 times greater than the calculated theoretical pressure (Table 2). This increase is due to the reduction of the contact area and impact of the surfaces.

Fig. 2b (part 2) shows the separation of the node from the contact surface since the contact stresses periodically become null. Furthermore, the associated spectrum, which is also periodic, resembles a shock spectrum (Fig. 3). Part 1 (Fig. 2b) shows the onset of instability as the amplitude of the stresses increases until it generates an impact phenomenon. Fig. 3 shows the Fourier transform preceding the separation phenomenon and the frequency of an unstable mode of the pad at about 20 kHz. As soon as the separation of the node from the beam contact surface occurs, periodic shocks appear at the interface (Fig. 2b, part 2). By using the Fourier transform (Fig. 3) it is possible to detect that this periodic shock leads to all the multiples of the fundamental frequencies of separation at 20 kHz (20, 40, 60, etc…). Finally, these results clearly show that the instability starts occurring on an unstable mode of the pad at 20 kHz and continues with a shock phenomenon whose fundamental periodicity is the frequency of the unstable mode. In our application, a finite element modal analysis of the pad at rest shows the existence of a pad modes around 20 kHz. This frequency, which corresponds to the unstable mode of the pad obtained in the temporal analysis, occurs at a friction coefficient greater than 0.2. The modal analysis does not take into account the beam which is assumed to be rigid since the pad has a much weaker Young's modulus than that of the steel beam. To prove this, the modes of the pad alone, with a fixed base, were calculated, as were those of the pad coupled to the deformable beam at rest. The mode of interest in the 20 kHz range is presented in Fig. 4.

As can be seen, the frequency and shape are only slightly dependent on the boundary conditions imposed by the beam. Consequently, for this geometry and kinematic situation, it appears justifiable to define a pad mode for which the vibrations are mainly concentrated in the pad,

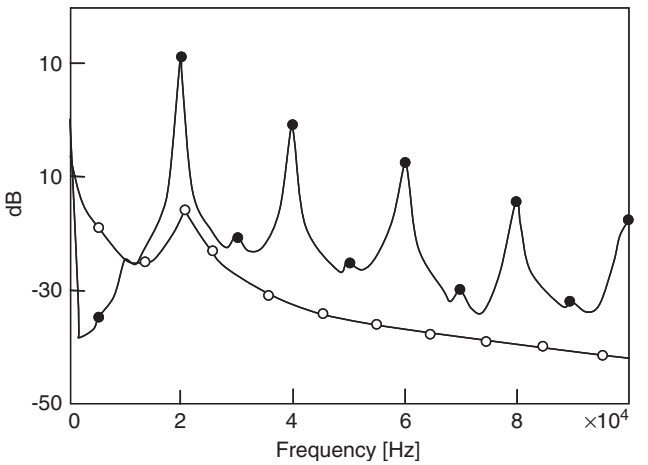

Fig. 3. Fourier transform of ○ part 1 and ● part 2 (Fig. 2b) of the normal contact stress of a node on the pad contact surface.

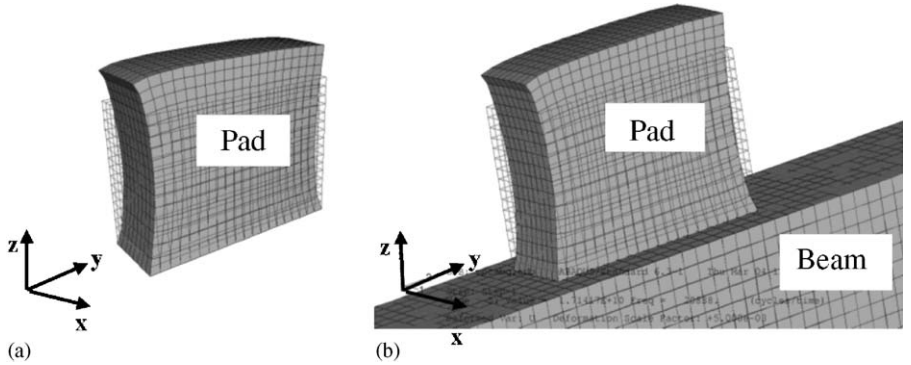

Fig. 4. Modes of pad: (a) with fixed base ($f = 21\,164$ Hz); (b) coupled to the deformable beam ($f = 20\,838$ Hz).

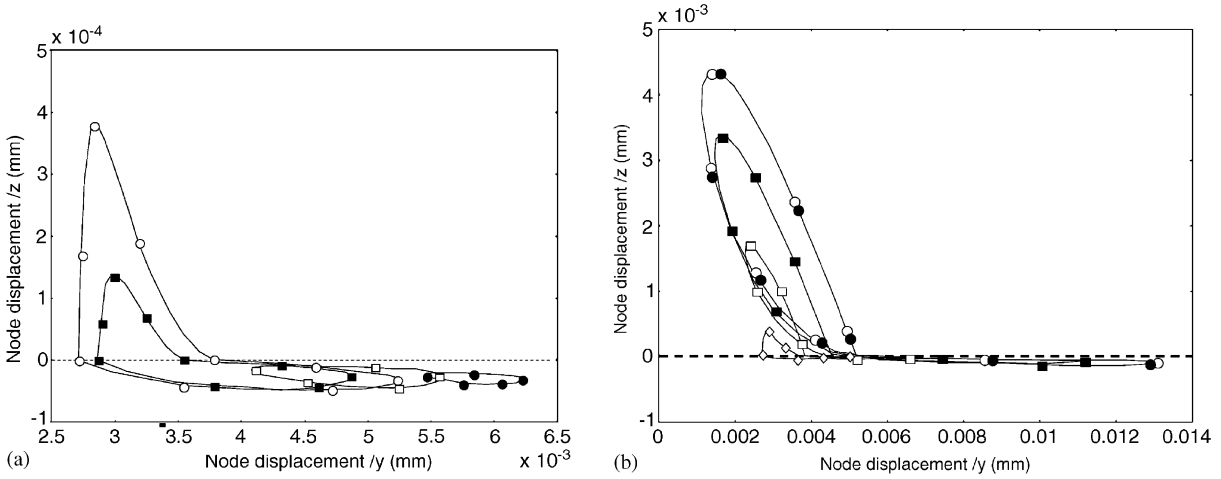

Fig. 5. Trajectory of a node situated on the pad contact surface for different beam speeds: (a) ○ $v = 0.1$ m/s, ■ $v = 0.075$ m/s, □ $v = 0.05$ m/s, ● $v = 0.025$ m/s; (b) ● $v = 10$ m/s, ○ $v = 2.5$ m/s, ■ $v = 0.5$ m/s, □ $v = 0.25$ m/s, ◇ $v = 0.1$ m/s.

whereas there are very few in the beam. Moreover, the reason this mode becomes unstable when the beam moves is because it exhibits a strong displacement component along the normal direction of the beam (z axis).

4.2. *Influence of beam speed*

The beam speed was changed for a given Coulomb friction coefficient ($\mu = 0.5$) and a normal applied force ($F = 135$ N, $P_{th} = 0.45$ MPa). In Fig. 5, for speeds lower than 0.05 m/s, the pad is in full contact with the beam and the instability is of the stick–slip type. The normal contact stress (Fig. 6) of a node situated on the pad contact surface due to this phenomenon oscillates around a value of 1.5 MPa, i.e. about three times the theoretical pressure. Distribution of the normal and

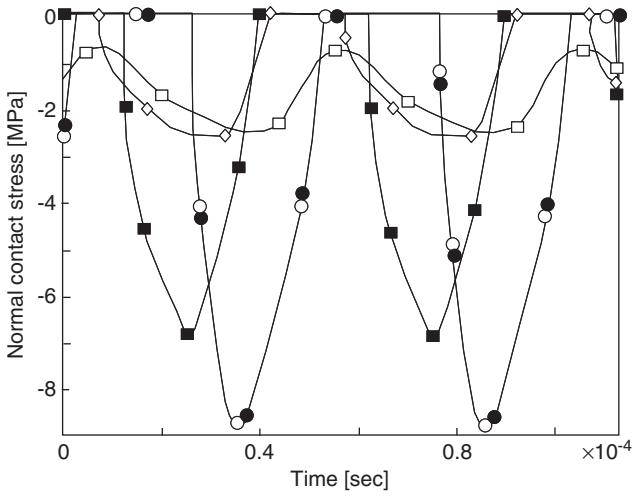

Fig. 6. Normal contact stress of a node situated on the pad contact surface for different beam speeds, ● $v = 10\,\mathrm{m/s}$, ○ $v = 2.5\,\mathrm{m/s}$, ■ $v = 0.5\,\mathrm{m/s}$, ◇ $v = 0.1\,\mathrm{m/s}$, □ $v = 0.05\,\mathrm{m/s}$.

tangential contact stresses are addressed in Refs. [23,29]. The separation of the contact surface from the pad starts to occur for speeds above 0.075 m/s. In this case sliding, sticking and separation of the pad contact zones occur. By increasing the speed, this separation phenomenon continues to increase until reaching a speed (in our case $v = 2.5\,\mathrm{m/s}$) at which the trajectory stabilises. This phenomenon affects the normal contact stress values, which can reach up to 20 times the theoretical pressure. As for the trajectory, the normal contact stress stabilizes when the speed increases beyond 2.5 m/s. The normal acceleration for the pad face (cf. Fig. 1) is shown in Fig. 7.

The amplitude of the acceleration increases with speed, as was the case for the normal contact stress (Fig. 6) and trajectory up to 2.5 m/s, and stays constant afterwards. The Fourier transform of the acceleration of both pad and beam face is produced at the same frequency (Fig. 8) at both low speeds (stick–slip in the contact interface) and high speeds (stick–slip–separation in the contact interface).

The frequency of the peaks of these instabilities does not vary with speed, rather it is the amplitude of the peaks corresponding to the noise level that changes. Strong levels of acceleration can be observed since the amplitude of vibration for the peak at 20 kHz reaches 90 dB for a speed of 0.1 m/s, corresponding to an acceleration of $10\,000g$. However, the low accelerations levels are due to the boundary conditions imposed on the beam. In the braking application where a rotating circular disc is considered, the levels of acceleration on the two bodies (disc/pad) are similar [23]. A link can be found between the impact frequency given by the normal contact stress and the frequency of the acceleration spectrums.

4.3. *Influence of the theoretical pressure applied to the pad*

The theoretical pressure ($P_{\mathrm{th}} = F/S$) imposed on the pad was changed for a given Coulomb friction coefficient ($\mu = 0.5$) and beam speed ($v = 5\,\mathrm{m/s}$). For values of theoretical pressures less

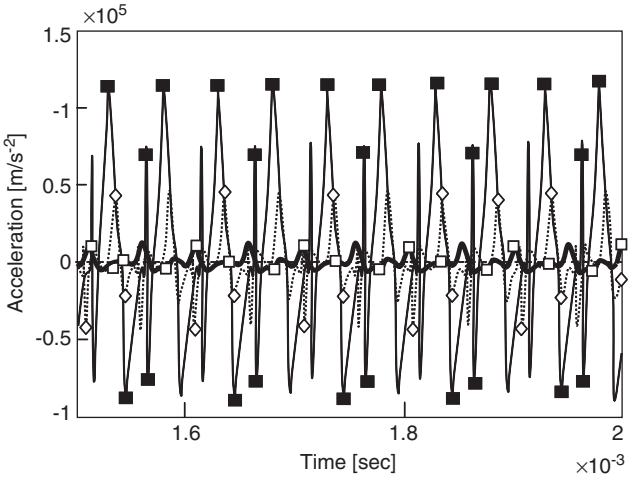

Fig. 7. Acceleration of the pad face 1 (cf. Fig. 1) for different beam speeds, ■ $v = 0.5\,\mathrm{m/s}$, ◇ $v = 0.1\,\mathrm{m/s}$, □ $v = 0.025\,\mathrm{m/s}$.

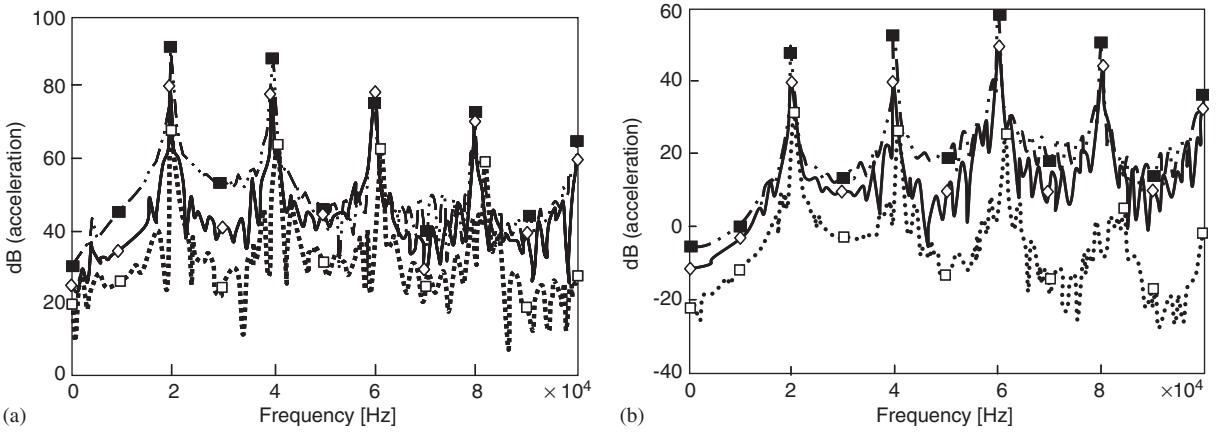

Fig. 8. Fourier transform of the acceleration of face: (a) 1 (pad); (b) 2 (beam) (cf. Fig. 1) for different beam speeds, ■ $v = 0.5\,\mathrm{m/s}$, ◇ $v = 0.1\,\mathrm{m/s}$, □ $v = 0.025\,\mathrm{m/s}$.

than 2 MPa, slip–separation occurs at contact level with a maximum displacement according to z of 15 μm (Fig. 9a). By raising the pressure (P_{th} values between 2 and 5 MPa), the pad contact zones begin to stick to the beam surface and more significant separations occur. For pressures above 5 MPa the magnitude of separation diminishes until all pad contact surface stick–slip and separation ceases.

This phenomenon also has repercussions on the normal contact stresses (Fig. 9b) where, for a theoretical pressure P_{th} less than 2 MPa, there is a regular increase of the normal contact stress with no change of frequency. As soon as sticking occurs in the pad contact zones ($P_{\mathrm{th}} \geqslant 2\,\mathrm{MPa}$), the contact time (sticking + sliding) increases without changing the frequency of impact. As shown

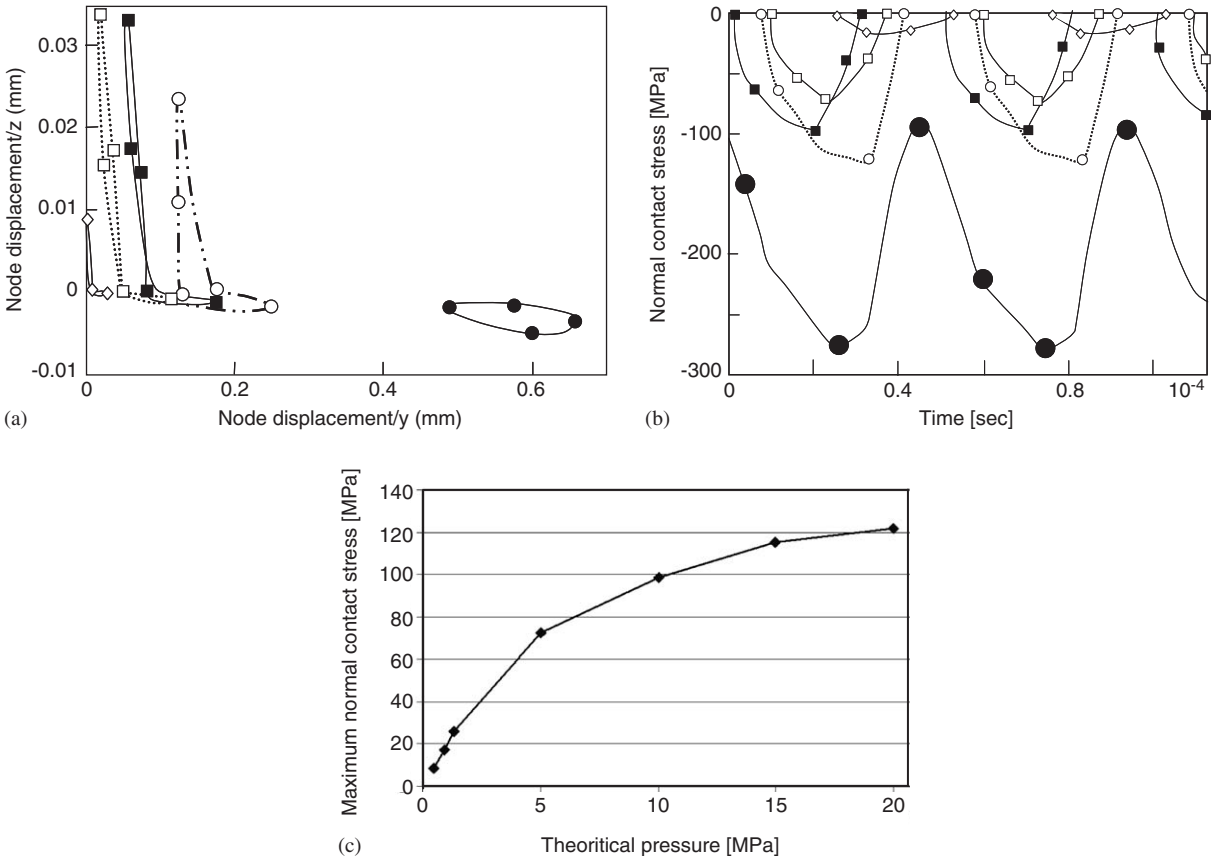

Fig. 9. (a) Trajectory; (b) normal contact stress; and (c) (σ_n)_max on the pad contact surface for different values of theoretical pressure, ● $P_{th} = 50$ MPa, ○ $P_{th} = 20$ MPa, ■ $P_{th} = 10$ MPa, □ $P_{th} = 5$ MPa, ◇ $P_{th} = 0.9$ MPa.

in Fig. 9c, increasing the theoretical pressure also increases the maximum normal contact stress which in turn correlates with an increase in the number of pad contact zones that stick. Once separation ceases ($P_{th} \geqslant 5$ MPa), the stress varies due to stick–slip type instabilities.

Consequently, the vibrations generated are greater, and so are the amplitudes, as can be seen in Fig. 10. As in the case of the variation of beam speed, we observed that the imposed theoretical pressure does not significantly affect the peak frequencies, though it does affect their amplitudes. In the small pressure range, the increase of these static pressures leads to an increase of the peak amplitudes. At higher pressures, when the pad contact sticking zone area increases, the amplitude of the peaks tends to stabilize as do the maximal normal contact stresses.

4.4. *Influence of Coulomb's friction coefficient* μ

Coulomb's friction coefficient at the surface of the beam/pad contact was changed for an imposed normal force ($F = 135$ N, $P_{th} = 0.45$ N) and a given speed ($v = 5$ m/s). Its influence on

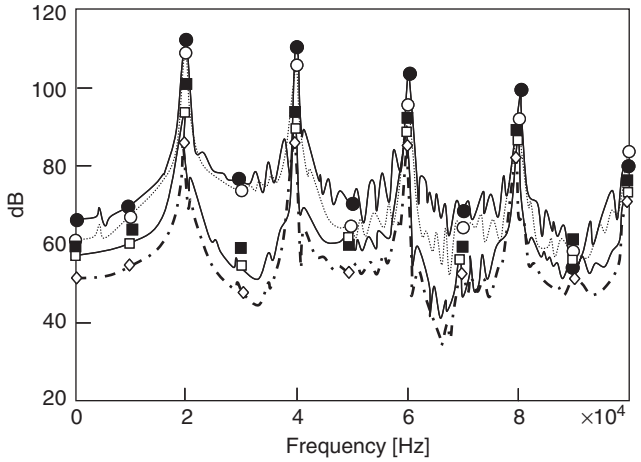

Fig. 10. Fourier transform of the pad face 1 (cf. Fig. 1) for different theoretical pressure values, ● $P_{th} = 10\,MPa$, ○ $P_{th} = 5\,MPa$, ■ $P_{th} = 1.35\,MPa$, □ $P_{th} = 0.9\,MPa$, ◇ $P_{th} = 0.45\,MPa$.

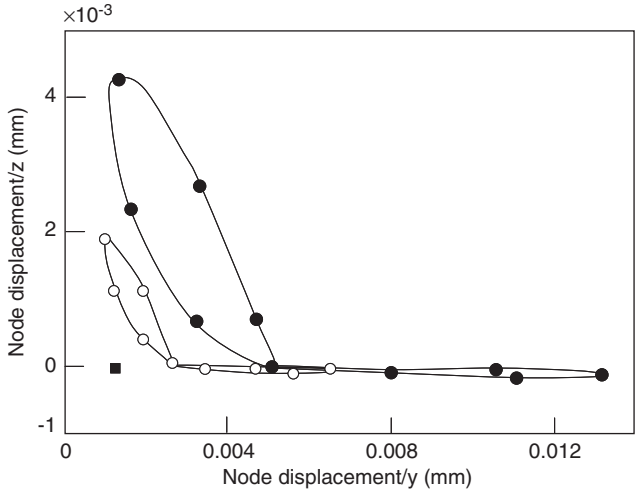

Fig. 11. Trajectory of a node on the pad contact surface for different values of Coulomb's friction coefficient, ● $\mu = 0.5$, ○ $\mu = 0.3$, ■ $\mu = 0.1$.

trajectory and normal contact stress is shown in Figs. 11 and 12 for a node situated on the pad contact surface.

It should be noted that a threshold friction coefficient exists above which instabilities are generated at the contact surface. For low friction coefficients the pad slides (constant contact stresses) on the beam and no instability phenomenon occurs (Fig. 11b). Above a friction value of 0.2, instabilities (stick–slip–separation of the contact surfaces) begin to occur and the normal contact stress increases (Fig. 12). The absence of instabilities indicates low acceleration values

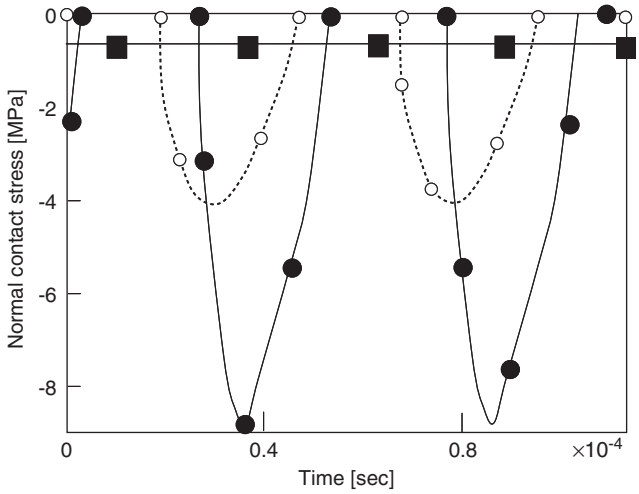

Fig. 12. Variation of the normal contact stress of a node on the contact surface of the pad as a function of Coulomb's friction coefficient, ● $\mu = 0.5$, ○ $\mu = 0.3$, ■ $\mu = 0.1$.

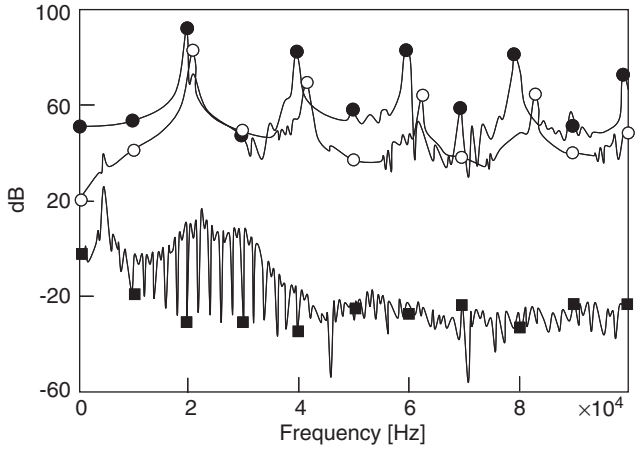

Fig. 13. Fourier transform of the acceleration of pad face 1 (cf. Fig. 1) for different values of Coulomb's friction coefficient ● $\mu = 0.5$, ○ $\mu = 0.3$, ■ $\mu = 0.1$.

either on the pad or on the beam. Once instabilities occur, the amplitude of acceleration increases at the same time as the friction coefficient. Fig. 13 shows the Fourier transform obtained for different values of Coulomb's friction coefficient.

A peak of low amplitude and a frequency of about 5 kHz are reached for low friction coefficient values ($\mu \leqslant 0.2$) where there are no instabilities. This spectrum corresponds to that of a sliding noise generated by the pad surface in stationary sliding contact on the moving beam surface. The spectrum's low amplitude and frequency depend on the mechanical and geometrical characteristics of the two materials in contact.

Instabilities generate steady-self pulses propagation at high frequencies in our model. The highest peak in this application is about 20 kHz, which, as in previous cases, corresponds to the frequency of impacts between the contact surfaces. Above this friction coefficient threshold value, its increase coincides with that of the acceleration amplitude and to a decrease in the frequency of the peaks.

4.5. Influence of the pad dimensions

The pad dimensions were changed from $10 \times 30 \times 20$ to $10 \times 15 \times 10$ mm (width × length × height) for a given speed ($v = 5$ m/s) and an imposed normal force ($F = 135$ N, $P_{th} = 0.45$ N). Reducing pad dimensions leads to reduced separations (from 4 to 1 μm) and normal contact stress (9–5 MPa) of the pad nodes in contact with the beam and an increase of impact frequency (Fig. 14).

Using a smaller pad leads to an increase in the frequency of the peaks, from 20 to 40 kHz. The spectrum therefore moves towards high frequencies (Fig. 15). Instability then occurs for a pad mode of 40 kHz.

4.6. Influence of Young's modulus

Simulations of the pad with different Young's moduli were performed for an imposed normal force ($F = 135$ N, $P_{th} = 0.45$ MPa) and a given speed ($v = 5$ m/s). The trajectory and normal contact stress of a node of the contact surface of the pad are shown in Fig. 16.

It can be seen that there is a threshold value for Young's modulus ($E > 50\,000$ MPa) above which instability ceases. By increasing Young's modulus, the separation decreases until it disappears and the situation changes from unstable to stable when the pad slides on the beam. As demonstrated by Adams [15,16], these instabilities are not possible for certain combinations of

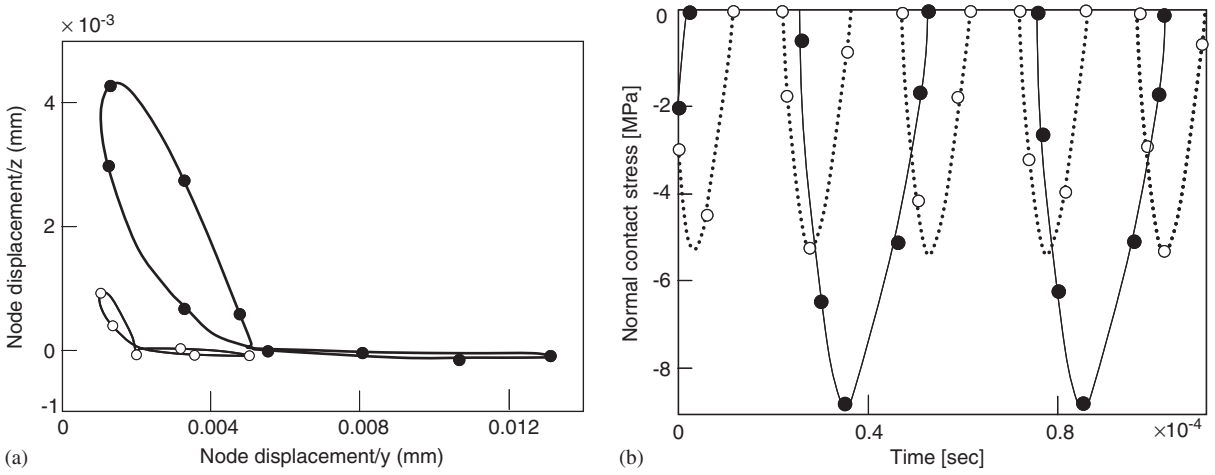

Fig. 14. (a) Trajectory and (b) normal contact stress of a pad node for pad dimensions ● $10 \times 30 \times 20$ and ○ $10 \times 15 \times 10$ (width × length × height).

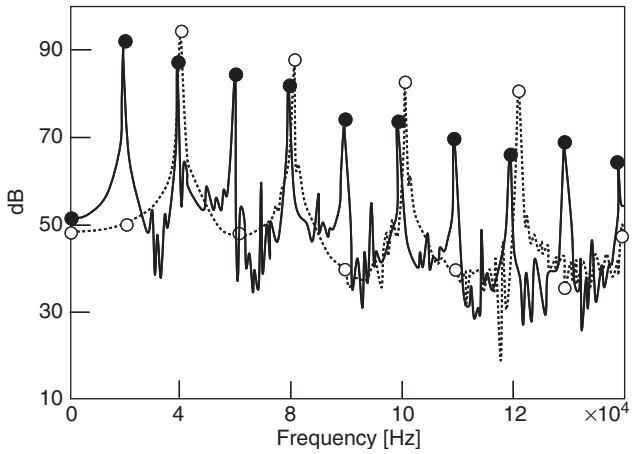

Fig. 15. Fourier transform of the acceleration of pad face 1 (cf. Fig. 1) for pad dimensions ● $10 \times 30 \times 20$ and ○ $10 \times 15 \times 10$ (width × length × height).

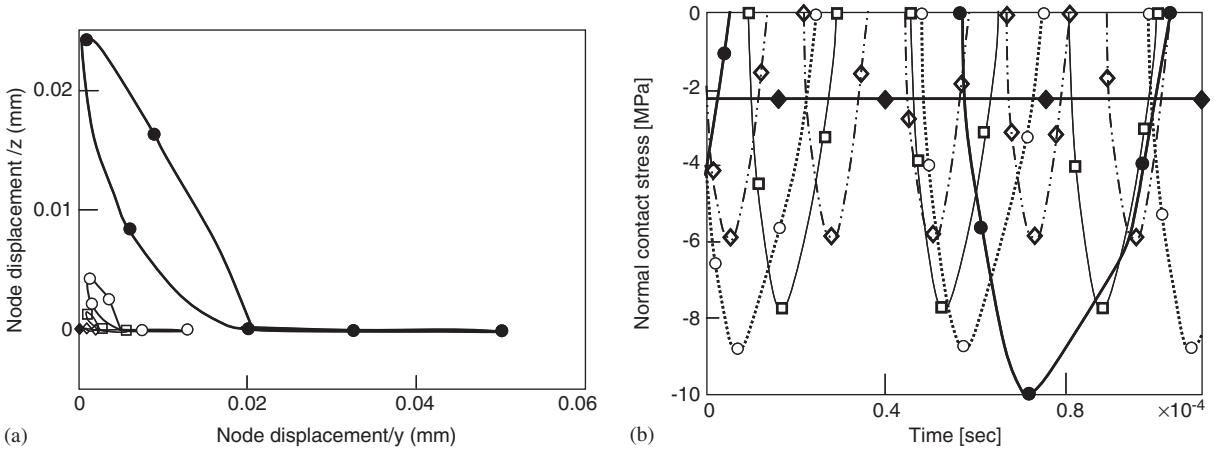

Fig. 16. (a) Trajectory and (b) normal contact stress of a pad node for different values of the pad's Young's modulus, ● $E = 2000$ MPa, ○ $E = 7000$ MPa, □ $E = 14\,000$ MPa, ◇ $E = 35\,000$ MPa, ◆ $E = 50\,000$ MPa.

materials. Reducing separation (increased Young's modulus) in the unstable zone leads to a reduction of normal contact stress on the one hand, but an increase of impact frequency on the other. The Fourier transform of the acceleration of a pad face whose amplitude is decreased by increasing Young's modulus is shown in Fig. 17.

As for the normal contact stress, lower amplitudes and higher frequencies can be obtained by increasing Young's modulus. The spectrum displaces towards high frequencies and a the amplitude is attenuated rapidly in cases where instability exists. These instabilities all start from a characteristic pad mode that changes as a function of Young's modulus. A stable situation of pure sliding exists above the threshold value, the former being characterized by peaks of low amplitude

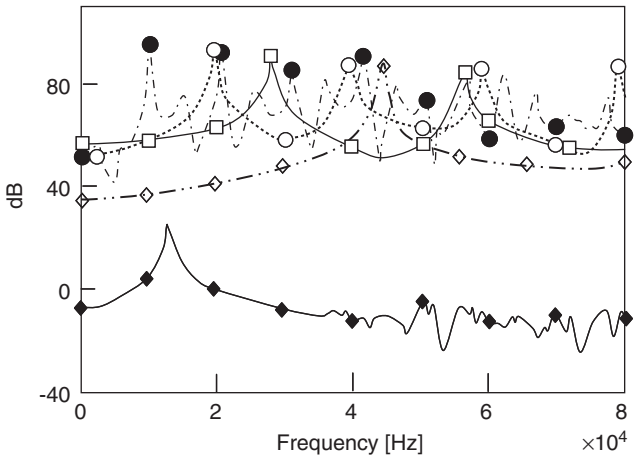

Fig. 17. Fourier transform of the acceleration of pad face 1 (cf. Fig. 1), for different Young's modulus ● $E = 2000$ MPa, ○ $E = 7000$ MPa, □ $E = 14\,000$ MPa, ◇ $E = 35\,000$ MPa, ◆ $E = 50\,000$ MPa.

that are related to sliding noise. Finally the rigidity of the pad contributes towards decreasing the both instabilities and the squealing phenomenon. Obviously, a Young's modulus of 2000 MPa makes it possible to predict a peak acceleration of about 10 kHz, and thus perceptible to the human ear.

5. Conclusions

This article has focused in particular on the influence of the main parameters involved in the instability phenomena generated by beam/pad friction contacts. The simulation of two bodies (pad and beam) sliding with a constant friction coefficient and a smooth surface has highlighted the occurrence of vibrations. The dynamic coupling between the volume and surface of the contact bodies leads to a contact surface composed locally of zones in contact and separated zones. Local separation of the pad and beam contact surface, leading to local normal impacts and increased high vibration may involve squealing. Apart from the friction coefficient, an essential parameter capable of activating instability, we have demonstrated the influence of beam speed, the contact pressure applied, the dimension of the pad and its Young's modulus. In the case of the model used here, rigidity contributes towards attenuating the instabilities and therefore the noise radiated. It was shown that the instability starts at a pad mode. In our model, this mode can be estimated by a finite element modal analysis of the pad while neglecting the beam, which represents a clamped boundary condition. During instability, steady-self pulses in the form of stick–slip–separation cause a periodic impact whose fundamental frequency remains that of an unstable mode at the source of the vibratory divergence. This impact then occurs at the interface, thus periodically separating the contact surfaces from each other. The Fourier transform of the squealing noise shows a spectrum of peaks whose harmonic diversity depends on the separation of the contact node and on the temporal evolution of the normal contact stress.

Acknowledgements

The 3D braking simulations were mostly carried out on the computer of the Centre Informatique National de l'Enseignement Supérieur.

References

[1] M. Godet, The third body approach, a mechanical view of wear, *Wear* 100 (1984) 437–452.
[2] Y. Berthier, Tribologie science carrefour, *Journées Européenne du Freinage (JEF)* (1992) 26.
[3] Y. Berthier, S. Descartes, Rheology and flows of solid third bodies: background and application to an $MoS_{1.6}$ coating, *Wear* 252 (2002) 546–556.
[4] H.R. Mills, Brake squeak: first interim report, Report No. 9000B, Institution of Automobile Engineers, Automobile Research Committee, 1938.
[5] M.R. North, Disc brake squeal, in: *Braking of Road Vehicles*, Loughborough, UK, 1976.
[6] J. Hulten, Friction phenomena related to drum brake squeal instabilities, *ASME Design Engineering Technical Conferences*, *Sixteenth Biennial Conference on Mechanical Vibration and Noise*, ASME, Sacramento, 1997.
[7] J. Hulten, Lining-deformation-induced modal coupling as squeal generator in a distributed parameter disc brake model, *Journal of Sound and Vibration* 254 (1) (2002) 1–21.
[8] R.T. Spurr, A theory of disc brake squeal, *Proceedings of the Automobile Division, Institution of Mechanical Engineers* 61–62 (1) (1961) 33–52.
[9] N. Milner, An analysis of disc brake squeal, SAE 780332, 1978.
[10] S.W.E. Earles, M.N.M. Badi, On the interaction of two-pin-disc system with reference to the generation of disc brake squeal, SAE 780332, 1978.
[11] S.W.E. Earles, M.N.M. Badi, Oscillatory instabilities in a double pin and disc undamped system: a mechanism of disc-brake squeal, *Proceedings of the Institution of Mechanical Engineers* 198 (1984) 43–50.
[12] S.W.E. Earles, C.K. Lee, Instabilities arising from the frictional interaction of pin disc system resulting in noise generation, *Journal of Engineering for Industry, Transaction of the ASME* 98 (1976) 81–86.
[13] H. Murakami, N. Tsunada, T. Kitamura, A study concerned with a mechanism of disc-brake squeal, SAE 841233, 1984.
[14] A. Akay, Acoustics of friction, *Journal of the Acoustic Society of America* 111 (4) (2002) 1525–1548.
[15] G.G. Adams, Self-excited oscillations of two elastic half-spaces sliding with a constant coefficient of friction, *ASME Journal of Applied Mechanics* 65 (1995) 867–872.
[16] G.G. Adams, Steady sliding of two elastic half-spaces friction reduction due to interface stick–slip, *ASME Journal of Applied Mechanics* 65 (1998) 470–475.
[17] F.M.F. Simões, J.A.C. Martins, Instability and ill-posedness in some friction problems, *International Journal of Engineering Science* 36 (1998) 1265–1293.
[18] A. Cochard, J.R. Rice, Fault rupture between dissimilar materials: ill-posedness, regularization, and slip-pulse response, *Journal of Geophysical Research* 105 (2000) 891–907.
[19] K. Ranjith, J.R. Rice, Slip dynamics at the interface between dissimilar materials, *Journal of the Mechanics and Physics of Solids* 49 (2001) 341–361.
[20] Q.S. Nguyen, Instability and friction, *Comptes Rendus Mecanique* 331 (1) (2003) 99–112.
[21] A. Oueslati, Q.S. Nguyen, L. Baillet, Stick–slip–separation waves in unilateral and friction contact, *Comptes Rendus Mécanique* 331 (1) (2003) 133–140.
[22] F. Moirot, Q.S. Nguyen, A. Oueslati, An example of stick–slip and stick–slip–separation waves, *European Journal of Mechanics—A/Solids* 22 (1) (2003) 107–118.
[23] L. Baillet, S. D'errico, V. Linck, B. Laulagnet, Y. Berthier, Finite element simulation of dynamic instabilities in frictional sliding contact, *Journal of Tribology* 127 (3) (2005) 652–657.
[24] L. Baillet, H. Walter, M. Brunet, A 3D contact algorithm for explicit dynamic F.E. code applied to the ironing process, *Metal Forming*, Cracovie, 2000, pp. 141–147.

[25] L. Baillet, T. Sassi, Finite element method with Lagrange multipliers for contact problems with friction, *Comptes Rendus Mécanique* 334 (1) (2003) 917–922.
[26] N.J. Carpenter, R.L. Taylor, M.G. Katona, Lagrange constraints for transient finite element surface contact, *International Journal for Numerical Methods in Engineering* 32 (1991) 103–128.
[27] B. Laulagnet, Sound radiation by a simply supported unbaffled plate, *Journal of the Acoustic Society of America* 103 (5) (1998).
[28] L. Baillet, Y. Berthier, S. Descartes, Modelling of the vibrations induced by friction: experimental visualisation and identification of the relays between the first bodies and the third body, *Journées Européenne du Freinage* 1 (2002) 181–188.
[29] L. Baillet, S. D'errico, Y. Berthier, Influence of sliding contact local dynamics on macroscopic friction coefficient variation, *REEF* 14 (2/3) 305–321.
[30] M. Eriksson, S. Jacobsen, F. Bergman, Influence of disc topography on generation of brake squeal, *Wear* 225–229 (1999) 621–628.
[31] M. Eriksson, S. Jacobsen, F. Bergman, Surface characterisation of brake pads after running under silent and squealing conditions, *Wear* 232 (1999) 163–167.
[32] J. Weertman, Unstable slippage across a fault that separate elastic media of different elastic constants, *Journal of Geophysical Research* 85 (1980) 1455–1461.
[33] Y. Ben-Zion, Dynamic ruptures in recent models of earthquake faults, *Journal of the Mechanics and Physics of Solids* 49 (9) (2001) 2209–2244.